JOURNAL OF GEOPHYSICAL RESEARCH, VOL. 105, NO. B4, PAGES 8243–8262, APRIL 10, 2000

# Anomalous seafloor spreading of the Southeast Indian Ridge near the Amsterdam-St. Paul Plateau

Daniel S. Scheirer, Donald W. Forsyth, James A. Conder, Michael A. Eberle[1], and Shu-Huei Hung[2]

Department of Geological Sciences, Brown University, Providence, Rhode Island

Kevin T. M. Johnson

Bishop Museum, Natural Sciences, Honolulu, Hawaii

David W. Graham

College of Oceanography and Atmospheric Sciences, Oregon State University, Corvallis

**Abstract.** The Amsterdam-St. Paul Plateau is bisected by the intermediate-rate spreading Southeast Indian Ridge, and numerous geophysical and tectonic anomalies arise from the interactions of the Amsterdam-St. Paul hotspot and the spreading center. The plate boundary geometry on the hotspot platform evolves rapidly (on timescales <1 Myr), off-axis volcanism is abundant, the seafloor does not deepen away from the axis, and transform faults do not have fracture zone extensions. Away from the hotspot platform the ridge-transform geometry is typical of mid-ocean ridges globally. In contrast, the Amsterdam-St. Paul Plateau spreading segments are shorter, they often overlap each other significantly, and the intervening discontinuities are smaller, more ephemeral, and more migratory. Abyssal hills are smaller and less uniform on the hotspot platform than on neighboring spreading segments. From gravity and isostasy analysis the average thickness of the platform crust is ~10 km, approximately 50% thicker than that of typical oceanic crust. Most of the isostatic compensation of the hotspot plateau occurs at the Moho or within the lower crust, and the effective elastic thickness of the plateau lithosphere is ~1.6 km, less than half that of adjacent spreading segments. Away from the platform some transform faults contain intratransform spreading centers; on the platform the two transform faults have valleys which may be depocenters for abundant axial or off-axis volcanism and mass wasting. Although not well-constrained by magnetics coverage, the Amsterdam-St. Paul hotspot appears to have been "captured" by the Southeast Indian Ridge, enhancing crustal production at the ridge since about 3.5 Ma. Prior to this time the hotspot formed a line of smaller, isolated volcanoes on older Australian plate. The underlying cause for the present-day crustal accretion anomalies is the effect of melt generation from separate sources of mantle upwelling (due to plate spreading and the hotspot) which has a consequent effect of weakening the lithosphere.

## 1. Introduction

The interactions between hotspots and mid-ocean ridges have profound effects on the formation of oceanic crust and lithosphere. The Iceland hotspot situated atop the northern Mid-Atlantic Ridge is the type example of this interaction in the present-day, and ridge-centered hotspots in the past have created symmetric aseismic ridges in every ocean basin. Hotspots situated away from mid-ocean ridges have varying degrees of compositional and tectonic influence on the crustal accretion which occurs at the spreading centers. While Iceland is one of the more robust hotspots according to a variety of global compilations [*Sleep*, 1990; *Schilling*, 1991], a less well-studied and smaller hotspot in the southern Indian Ocean, the Amsterdam-St. Paul (ASP) hotspot, is also very near a spreading center (Figure 1). The ASP hotspot has formed a volcanic massif approximately 150 km by 200 km in plan view which straddles the Southeast Indian Ridge (SEIR) [*Royer and Schlich*, 1988] (Plates 1 and 2). Sitting atop the plateau are two volcanic islands, Amsterdam and St. Paul, which formed as tholeiitic shields during the past 1 Myr [cf. *Upton*, 1992].

As the primary surface expressions of mantle upwelling, oceanic ridges and hotspots interact in a variety of ways. Significant topographic, geophysical, and geochemical anomalies have been identified along spreading centers which are in the vicinity of hotspots [e.g., *Talwani et al.*, 1971; *Vogt*, 1971; *Schilling*, 1973; *Morgan*, 1978]. Enhanced melting and crustal production occur at spreading centers underlain by hotspots due to more enriched mantle compositions and elevated temperatures; geochemical and geophysical anomalies may extend several hundred, to more than a thousand, kilome-

[1] Now at Fred Hutchinson Cancer Research Center, Seattle, Washington.

[2] Now at Princeton University, Princeton, New Jersey.



Paper number 1999JB900407.
0148-0227/00/1999JB900407$09.00

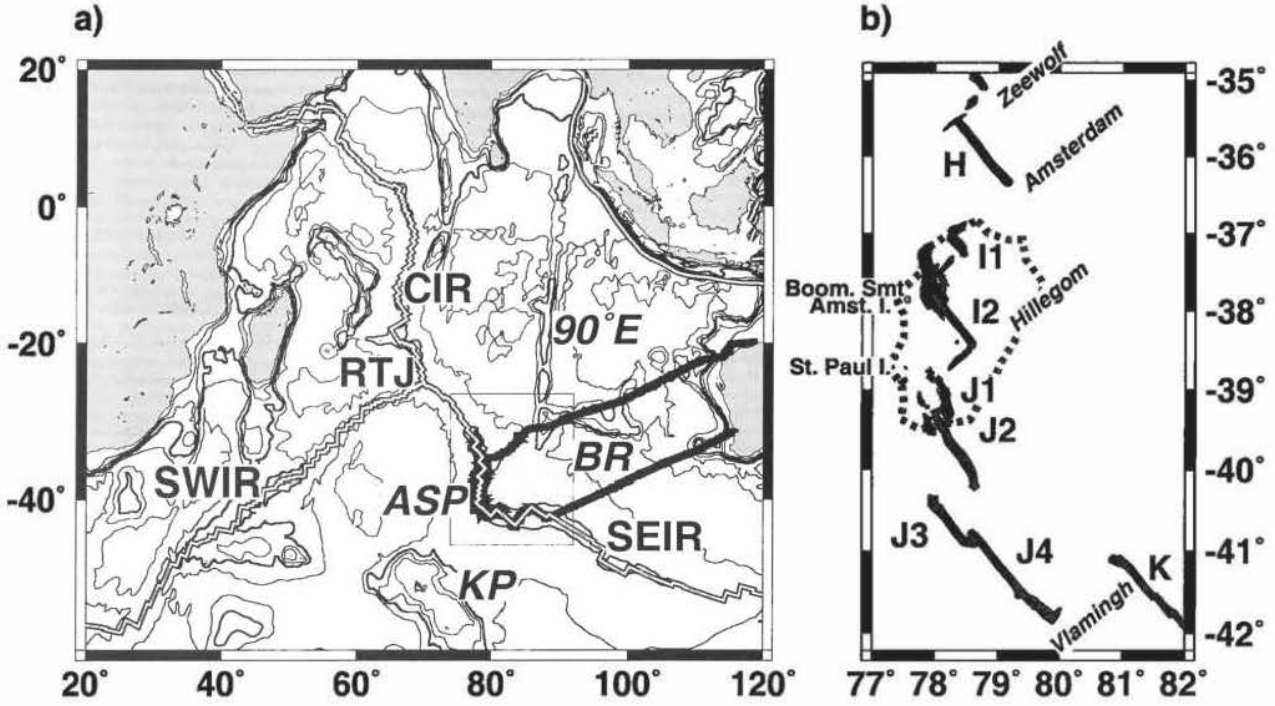


**Figure 1.** (a) The Indian Ocean spreading centers and selected hotspot features. Regional bathymetry is contoured every 1 km; thick line indicates the cruise track from Boomerang, Leg 6; shaded box indicates coverage area of Plate 1; and double line indicates the plate boundaries. (b) Study area illustrating ridge segment and discontinuity names and areas where reflective seafloor was imaged with side scan sonar. Lighter shaded areas are axial neovolcanic zones; darker shaded areas indicate high reflectivity off-axis. The dotted line outlines the ASP Plateau. 90°E, Ninetyeast Ridge; ASP, Amsterdam-St. Paul Plateau; BR, Broken Ridge; CIR, Central Indian Ridge; KP, Kerguelen Plateau; RTJ, Rodrigues Triple Junction; SEIR, Southeast Indian Ridge; SWIR, Southwest Indian Ridge.

ters away from the hotspot. The recognition that off-axis hotspots also produce anomalies at spreading centers led to models of preferential flow of hotspot material toward the spreading ridge, possibly along channels or along the base of the lithosphere which rises toward the spreading axis [*Vogt*, 1976; *Schilling*, 1985; *Kincaid et al.*, 1995].

Recently, the quantitative interactions between hotspots and oceanic ridges have been studied using a variety of approaches. Laboratory experiments have considered how mantle plumes disperse when situated both beneath a spreading center and off-axis [*Feighner and Richards*, 1995; *Kincaid et al.*, 1995]. In parallel efforts, theoretical and numerical modeling of on-ridge and off-ridge hotspots has been used both to understand the laboratory results and to constrain the properties of plumes which influence spreading centers in the Atlantic, Pacific, and Indian ocean basins [*Ribe et al.*, 1995; *Ito et al.*, 1996; *Ribe*, 1996; *Sleep*, 1996; *Ito et al.*, 1997; *Yale and Phipps Morgan*, 1998; *Ito et al.*, 1999]. The results of these studies indicate that the magnitude and lateral extent of hotspot influence increases with increasing plume flux and buoyancy (functions of plume dimension, ascent rate, and decreased density and viscosity values relative to nonplume mantle) and with decreasing spreading rate of the oceanic ridge. For off-axis plumes the degree of influence is inversely related to the distance to the spreading center, and it is greater when a ridge migrates away from a hotspot than when it migrates toward the hotspot.

This paper and its companion [*Conder et al.*, this issue] present results from the geophysical component of a cruise during Leg 6 of the R/V *Melville's* Boomerang Expedition, which surveyed and sampled rocks along a 1500-km stretch of the SEIR surrounding the ASP hotspot plateau [*Johnson et al.*, 1996; *Scheirer et al.*, 1996] (Figure 1). The petrologic influence of the ASP hotspot on the mid-ocean ridge basalts erupted at the SEIR is clear in the major element, trace element, and isotopic compositions [*Douglas et al.*, 1996; *Douglas Priebe*, 1998; *Graham et al.*, 1999; K. T. M. Johnson et al., Boomerang Seamount: An active expression of the Amsterdam-St. Paul hotspot, Southeast Indian Ridge, submitted to *Earth and Planetary Science Letters*, 1999, hereinafter referred to as Johnson et al., submitted manuscript, 1999]. This paper will concentrate on the morphology of the spreading center along this stretch of the SEIR and on the structure at depth which we can infer from gravity analysis. *Conder et al.* [this issue] present results from magnetics and seafloor morphology analysis on the nature and evolution of the plate boundary on the hotspot plateau, with comparisons to observations on Iceland.

## 2. Background

The SEIR is one of the three spreading centers which subdivides the Indian Ocean basin (Figure 1); spreading occurs between the Australian and Antarctic plates. Near the ASP Plateau, the SEIR spreads at a nearly constant, full-rate of 65 mm/yr, an intermediate value in the spectrum of mid-ocean ridge spreading rates. In the hotspot frame of reference the Antarctic plate is virtually stationary [*Gripp and Gordon*, 1990]. Thus the Australian plate moves to the northeast in the

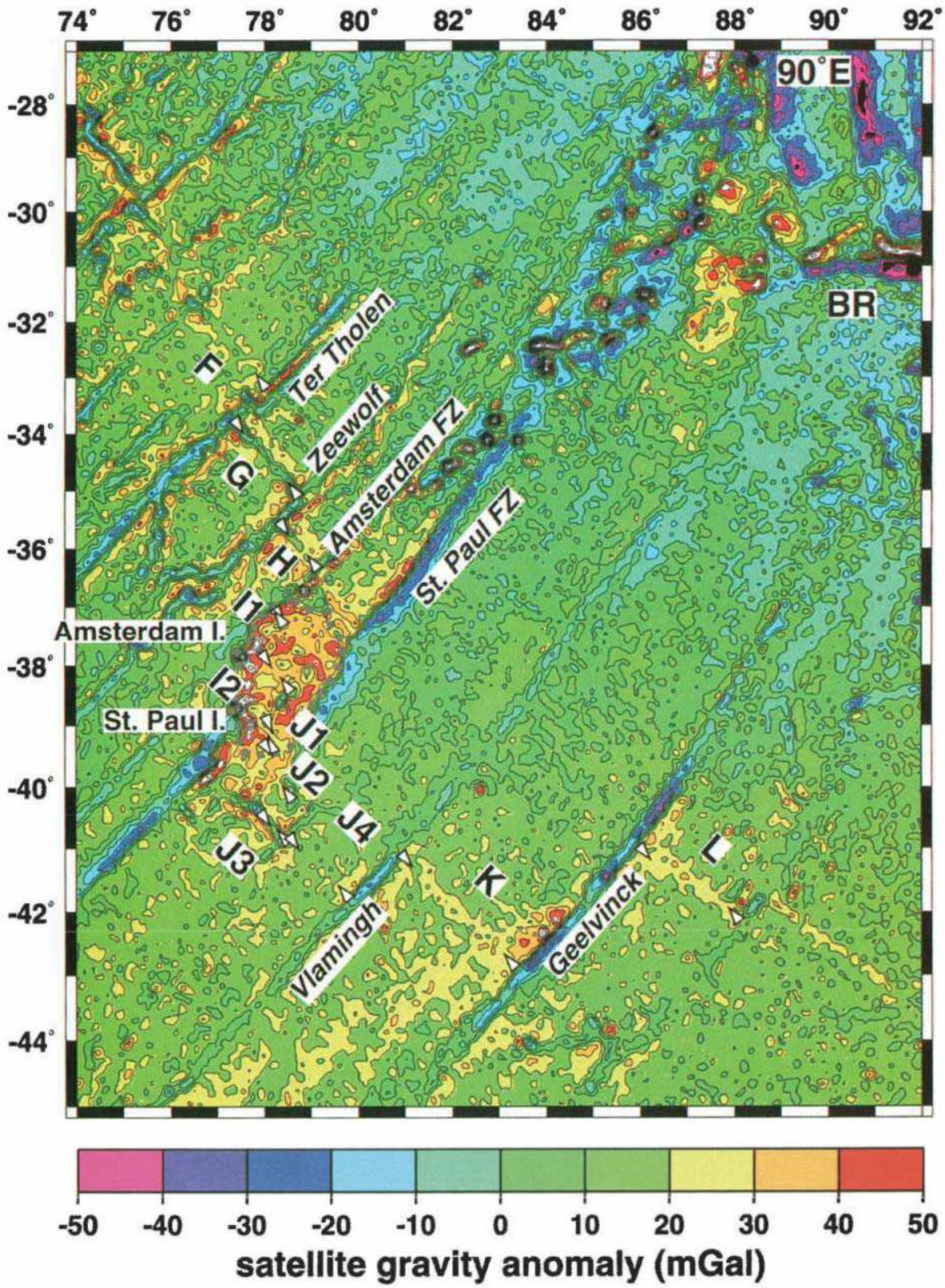


**Plate 1.** Free-air gravity anomalies of the study area contoured every 10 mGal, calculated from satellite altimetry data [*Sandwell and Smith*, 1997]. The spreading segments (F-L), major ridge axis discontinuities, and islands are labeled; the ends of the spreading segments in the study area are indicated with white arrow heads. Outline of the ASP platform is dotted gray line. The SW extent of the line of volcanoes thought to be the hotspot trace of the ASP plume is just below the Amsterdam FZ label. 90°E, Ninetyeast Ridge; BR, Broken Ridge.

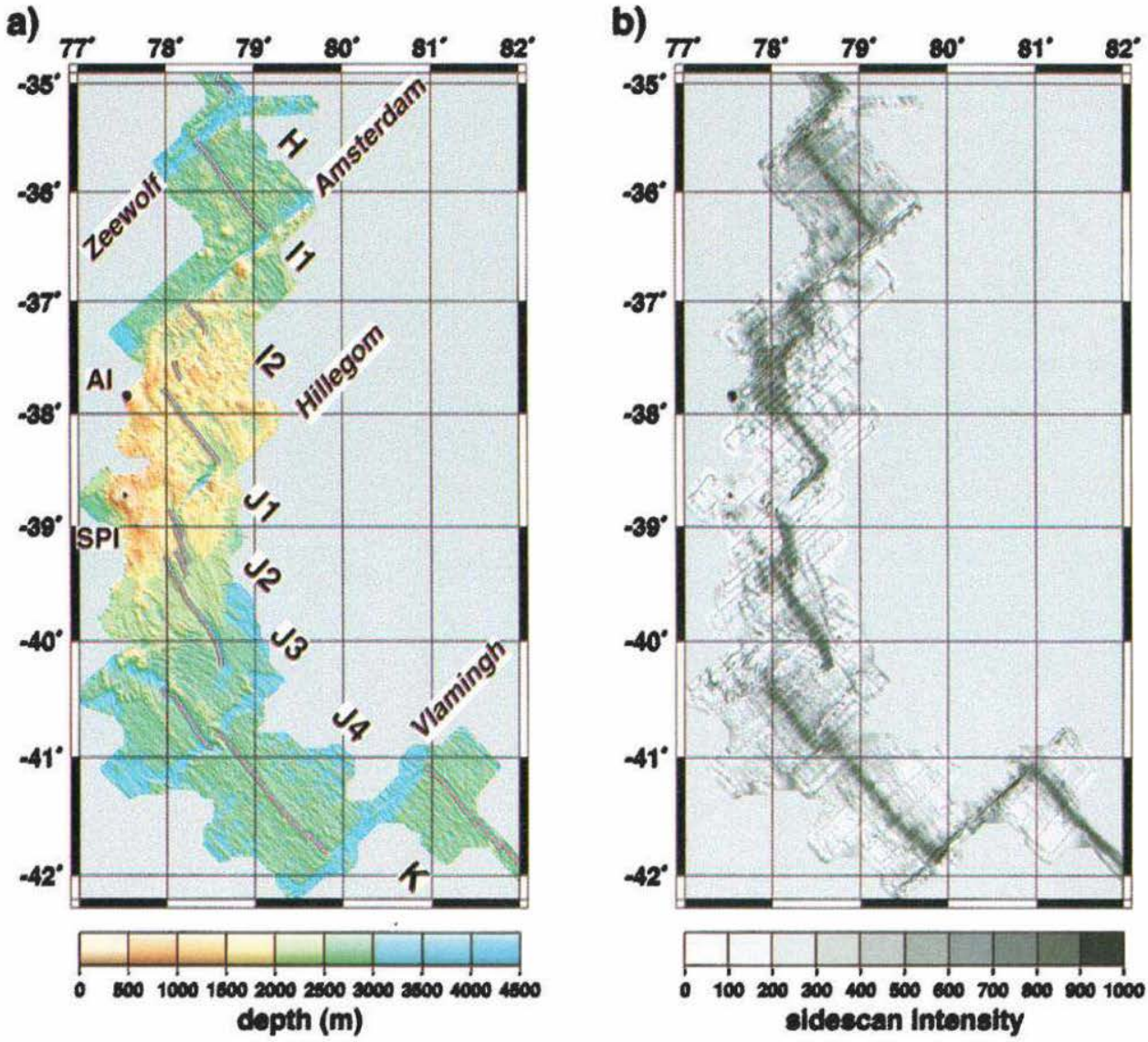


**Plate 2.** (a) Bathymetry and (b) side scan maps of the ASP platform and adjacent segments where we have significant off-axis coverage. Small data gaps in both of these gridded data sets have been filled using projection onto convex sets (POCS) interpolation [*Conder et al.*, this issue] to preserve the continuity of major features; Plates 3, 4, and 5 illustrate the true data coverage. Bathymetry has been artificially illuminated from the NE. For the side scan map, reflective seafloor, such as near the spreading segments, is shown by dark tones.

hotspot reference frame at the total opening rate of the SEIR, and the ridge axis itself migrates at half that rate (~32 mm/yr) over the hotspots.

The ASP Plateau can be delimited by the depth transition from 2300 to 2800 m, and it has an area in excess of 30,000 km$^2$ (Plate 2). Preexisting marine geophysical and rock compositional data are sparse for the ASP Plateau. A compilation of the prior underway bathymetry and magnetics data is presented by *Royer and Schlich* [1988], consisting mainly of track lines of opportunity in support of French scientific operations on the islands, plus a few systematic surveys collected over the past several decades. Gravity data were not collected on many of these cruises, nor are all of the cruise data sets publicly available. Prior to Boomerang Leg 6, very little multibeam bathymetry and no side scan data were available for this area. Comprehensive multibeam, geophysical, and petrologic studies were conducted in 1994/1995 along the ~2000-km-long section of the SEIR extending to the southeast of our study area; these extend to the Australian-Antarctic Discordance (AAD) and illustrate the gradient in axial morphology and other SEIR properties toward the discordance [*Cochran et al.*, 1997; *Goff et al.*, 1997; *Sempere et al.*, 1997; *Shah and Sempere*, 1998].

Both Amsterdam and St. Paul islands are on the Antarctic plate and are within 40 km of the nearest spreading segments. A line of submarine volcanoes to the northeast of the ASP Plateau appears to be the trace of the ASP hotspot (Plate 1) [*Sandwell and Smith*, 1997; *Mitchell and Livermore*, 1998]. On our outbound transit we crossed a number of these volcanoes. In these bathymetry data and the satellite gravity field the volcanoes are isolated and generally circular in plan view, with heights 1.5 to 3 km above the surrounding seafloor and basal diameters up to 40 km. The northeastern extent of this chain merges with the complex intersection of Broken Ridge and the Ninetyeast Ridge. Although seafloor in this spreading corridor has not been dated with magnetic anomalies [*Royer and Sandwell*, 1989], the geometry of the volcanoes and the adjacent fracture zones (along with their age offsets from prior times) suggest that the ASP hotspot stopped forming this chain on the Australian plate between 5 and 10 Ma and that its volcanism was intercepted by the SEIR, which had been migrating toward it. We surmise that once it was captured by the ridge, the hotspot was able to build a shallow platform by adding to the igneous accretion at the spreading center. The width of seafloor affected by volcanism from the hotspot when it was off-axis is considerably narrower than the along-axis dimension of the ASP Plateau (Plate 1). Currently, the locus of ASP hotspot volcanism appears to be entirely on the Antarctic plate, where it has formed the islands and other shallow portions of the ASP Plateau.

The larger, more distant, and longer-lived Kerguelen hotspot is also thought to influence the composition of some mid-ocean ridge basalts (MORB) collected along the SEIR [*Hamelin et al.*, 1986; *Dosso et al.*, 1988; *Storey et al.*, 1989]. The Kerguelen Archipelago is ~1150 km to the southwest of the nearest SEIR spreading segment, although MORB samples carrying the distinctive Kerguelen isotopic signature were collected near the center of the ASP Plateau, ~1400 km from the Kerguelen Island [*Hamelin et al.*, 1986]. The isotopic signatures of the ASP and Kerguelen hotspots are distinct, which discounts the hypothesis of a simple connection via a sublithospheric pipe between the large off-ridge Kerguelen hotspot and its potential near-ridge expression as the ASP Plateau [*Morgan*, 1978]. The Kerguelen anomaly does appear to influence the depth of the SEIR axis over distances thousands of kilometers in scale [*Ma and Cochran*, 1996]. Just to the east of the study area near 90°E, the SEIR has a depth shallower than 2500 m, and it deepens gradually to the southeast to depths >4500 m at the AAD, ~1500 km away [*Cochran et al.*, 1997; *Sempere et al.*, 1997]. To the northwest of 90°E, the SEIR axis also gradually increases in depth to >4000 m at the Rodriguez Triple Junction, ~2000 km to the northwest [e.g., *Dosso*, 1988]. The axial morphology also becomes more rift-like both toward the Rodriguez Triple Junction (Plate 1) and toward the AAD.

## 3. Data Set

During Boomerang Leg 6, we collected SeaBeam2000 multibeam bathymetry, side scan, underway gravity, magnetics, and P-code Global Positioning System (GPS) navigation data; we also collected rock samples from over 90 sites both on and off the spreading axis. The 120° SeaBeam2000 bathymetry swath yields a cross-track coverage ~3.4 times the water depth; the SeaBeam2000 side scan swath covers ~10% more area than the bathymetry swath. We acquired ~50% multibeam coverage off the platform, and by narrowing the track spacing on the platform we approached full coverage for much of this shallow area.

In general, the data quality was uniformly high, in large part due to the relatively calm seas encountered in all but a few days. To mitigate the effects of bathymetry noise, we developed a despiking algorithm for the multibeam bathymetry data which flagged as anomalous any beam whose depth was significantly (>40 m) different from the average depth of the same beam for the three preceding and three following pings. Because SeaBeam2000 data often have missing data near the edges of the swath where the spike anomalies are present, this algorithm was extended to look over five-ping and seven-ping half-width windows using correspondingly higher noise thresholds. After the despiking, the bathymetry data were edited by hand to delete any remaining outlier beams. This latter step was time consuming only for the few days when the ship pitched in heavy seas.

The raw SeaBeam2000 sonar records were converted to a 12-bit side scan format using the program sbextractss (D. Caress, personal comm.). Because of the high sonar levels returning from nadir positions and the systematic decrease in signal toward the edge of the swath, we devised an equalizing algorithm to reduce the systematic side scan amplitude variations across the swath. Tables of equalized histograms of side scan values, as a function of position within the swath, were calculated from a representative section of the seafloor survey to the south of the ASP Plateau. Raw side scan values were converted to their equalized counterparts via interpolations from these tables. This process equalizes across the swath both the average side scan value and the scatter of values, and maps created with these equalized data have much smaller artifacts related to the data collection geometry than their unprocessed counterparts.

The side scan data were particularly useful in delineating the axial neovolcanic zones and areas of recent off-axis volcanism. High side scan backscatter values are associated with slopes facing the ship (e.g., fault scarps or seamount flanks)

and with areas of seafloor which are rough at a length scale similar to the sonar wavelength of ~10 cm (e.g., unsedimented lava or debris flows). Reflective seafloor defines the axial neovolcanic zones; within ±3 km of the spreading axis the seafloor reflectivity is uniformly high everywhere. Reflectivity decreases out to distances of 10-15 km from the axis, where it reaches levels that decrease only slightly with increasing seafloor age. The decrease in seafloor reflectivity with age is largely due to the accumulation of sediment [e.g. *Mitchell*, 1993]. Reflective seafloor away from the spreading axis is thus interpreted to be a young surface, marking recent lava flows or unsedimented mass-wasted material. Using the near-axis seafloor reflectivity versus age behavior as a guide, flat patches of seafloor with the highest reflectivity are thought to arise from surfaces younger than ~0.1 Ma, and other reflective patches are thought to represent slightly older flows, still younger than ~0.4 Ma. We recovered glassy basalt samples with no appreciable sediment in rock cavities at all of the rock sampling sites located on relatively flat, highly reflective seafloor, both on-axis and off-axis; this is an important ground truth of the reflectivity/age relationship.

Gravity and magnetic field data were collected and processed conventionally. The high quality of the navigation brought about excellent repeatability of along-track anomalies for crossing lines. For the 98 gravity crossovers the root-mean-square (RMS) error was 1.9 mGal, with 90% of the data falling between -2.6 and 2.8 mGal. For the 54 magnetics crossover errors the RMS was 39 nT, with 90% of the data falling between -56 and 84 nT. We attribute some of the magnetics variability to diurnal variation, which reaches 20 nT in this area at this time of year [*Hitchman et al.*, 1998], and some to the very high magnetic field gradients associated with the shallow topography and recent volcanism of the ASP Plateau.

## 4. Segmentation of the SEIR

In the survey region the SEIR comprises 11 long-lived spreading segments ranging in length from about 50 to 300 km (Plates 1 and 2). We assign them lettered names based on their correspondence to the SEIR spreading corridors studied by *Royer and Schlich* [1988]. These corridors start with A at the Rodriguez Triple Junction (RTJ) and increase along the SEIR toward the east. Our survey encompasses the spreading center along part of corridor F and along all of corridors G through L (Plate 1). Because the present-day spreading center exhibits complexity at a finer scale than studied when this nomenclature was devised [*Royer and Schlich*, 1988], we append numbers to the two spreading segments in corridor I (I1 and I2), and we subdivide the J corridor into four segments (J1, J2, J3, and J4).

Twelve ridge axis discontinuities with offsets >10 km segment the spreading center in the study area (Table 1). A number of smaller deviations in the axial trace are also present, but their influence does not appear off-axis. The significant discontinuities range in size from the 310 km (nearly 9.5 Myr) offset Geelvinck transform fault to overlapping spreading centers 15 km across (~0.4 Myr).

The major transform faults of the current plate boundary existed in the past, at least since Anomaly 6 time (~20 Ma). The SEIR between the RTJ and the AAD has a nearly straight trace except for a significant (~400 km) deviation to the southwest between segments H and L (Figure 1 and Plate 1). The deviation was inherited, for the most part, from the shape of the breakup of Australia and Antarctica at Broken Ridge and the Kerguelen Plateau around 43 Ma [*Royer and Sandwell*, 1989]. The St. Paul fracture zone (Plate 1), which existed as a major discontinuity for much of the SEIR spreading history, is no longer active, although the much smaller-offset Hillegom transform near the center of the ASP hotspot platform is collinear with its trace. The Hillegom transform may be the current stage of an evolving transform which formed the St. Paul fracture zone [*Conder et al.*, this issue], but as described below, its recent evolution is complex.

Away from the ASP Plateau, the spreading segments and transform faults are perpendicular to each other, and the only nontransform offset is a small overlapping spreading center (OSC) between segments J3 and J4 at 40°50'S (Plate 3). This OSC is marked by deep, overlapping rift zones surrounding an anomalously shallow ridge. This contrasts with OSCs along faster spreading mid-ocean ridges, which are characterized by curving axial ridges surrounding an overlap basin. This unusual topography of the 40°50'S OSC suggests that while the plan view interaction of adjacent segments is similar among OSCs (related to the interactions of extensional cracks [e.g., *Pollard and Aydin*, 1984]), the thermal, structural, and dynamic

**Table 1.** Ridge Axis Discontinuities Having Offsets >10 km in the SEIR Study Area

| Name | Type | Latitude S | Longitude E | Offset, km (Ma) | Stepping Sense | Segments | Distance,* km (deg) |
|---|---|---|---|---|---|---|---|
| Ter Tholen | TF | 33°28' | 77°45' | 91 (2 7) | R | F/G | -401 (59.98) |
| Zeewolf | TF | 35°20' | 78°34' | 59 (1.8) | R | G/H | -203 (61.77) |
| Amsterdam | TF | 36°42' | 78°41' | 115 (3 5) | R | H/I1 | -89 (62 79) |
| Boomerang | TF | 37°24' | 78°14' | 50 (1.5) | R | I1/I2 | -62 (63.03) |
| N/A | NTD | 37°44' | 78°05' | 19 (0.6) | R | I2 | -45 (63.19) |
| Hillegom | TF | 38°40' | 78°18' | 70 (2.1) | R | I2/J1 | 42 (63.97) |
| N/A | NTD | 39°16' | 78°05' | 17 (0.5) | R | J1/J2 | 77 (64.29) |
| N/A | PR | 40°18' | 78°20' | 67 (2.0) | R | J2/J3 | 175 (65.17) |
| N/A | OSC | 40°48' | 78°35' | 15 (0.4) | L | J3/J4 | 230 (65.66) |
| Vlamingh | TF | 41°30' | 80°22' | 124 (3.8) | L | J4/K | 390 (67.10) |
| Geelvinck | TF | 42°00' | 84°35' | 311 (9.4) | L | K/L | 683 (69.74) |
| N/A | TF | 42°00' | 88°20' | 56 (1.7) | L | L/M | 921 (71.88) |

TF, transform fault; NTD, nontransform discontinuity; OSC, overlapping spreading center; PR, propagating rift; N/A, not available; L, left-stepping; R, right-stepping.

*Distance is measured along the SEIR axis, in kilometers southeast of Amsterdam Island, and in degrees from the NUVEL-1A pole of opening for Australia and Antarctica.

conditions of different spreading centers may produce opposite topographic effects in the vicinity of an OSC.

Two of the off-platform transform faults, the Zeewolf and Geelvinck (Table 1), contain intratransform spreading centers (ITSC). The ITSC segment within the Zeewolf transform fault is ~15 km long, is highly reflective, separates two transform fault strands, and has formed abyssal hill lineaments which are truncated by those strands (Plate 4). A dredge haul collected fresh, glassy basalt from the axis of the Zeewolf ITSC. The limited coverage of the Zeewolf transform prohibits an assessment of how long the ITSC has been active, although the existing data are consistent with a duration at least as long as the current age offset of the Zeewolf transform fault, 1.8 Myr. In addition to the high side scan reflectivity associated with ITSCs, off-platform transform faults also have elevated backscatter due to tectonized seafloor (Plates 3 and 4), and in some instances (especially for the Vlamingh transform, Plate 3b), recent lava flows appear to extend beyond the tips of spreading segments to the deeper, adjoining seafloor.

On the ASP Plateau, there are only two, short transform faults (Plate 2a). While left-lateral strike-slip earthquakes are associated with these features [e.g., *Dziewonski et al.*, 1991], their topographic expression is not as simple as for those of transforms away from the platform. The morphology of the Boomerang Transform (Plate 5) is a subtle, deep zone which is slightly oblique to the plate spreading direction and which separates the abyssal hills formed at segments I1 and I2. We classify this a transform fault because of the two left-lateral earthquake focal mechanisms which have been determined and because the seafloor fabric does not appear to be sheared as at nontransform discontinuities. The other transform fault, the Hillegom transform, has 2 km deep walls and is considerably deeper midway between the adjacent spreading segments than near the segment tips. Both the Boomerang and Hillegom transforms are associated with reflective seafloor which does not appear to arise solely from steep slopes (Plate 5). The source of the high reflectivity of the Hillegom transform may, in part, involve steep, ragged walls where sediment does not accumulate. However, some of the high reflectivity is present at the nearly flat base of the transform zone, suggesting that sediments have not accumulated on the present-day seafloor. This leads to the intriguing possibility that recent lava flows have ponded at the base of Hillegom transform; alternatively, mass wasting of the transform walls may bring about the high reflectivity. The Boomerang transform is associated with an extensive area of high reflectivity (Plate 5b). In this case the large Boomerang Seamount [Johnson et al., submitted manuscript, 1999] and spreading segments of I2 are nearby, so the deep associated with the Boomerang transform may form a volcanic depocenter for these volcanically active areas.

If volcanic activity is associated with the two active transforms on the ASP Plateau, this may explain another characteristic which they share: the absence of inactive fracture zone traces. The southwestern extensions of the transform faults intersect the volcanic massifs associated with Amsterdam and St. Paul islands (Plate 2), and the northeastern extensions do not disrupt the seafloor (Plate 5), as would be expected if the transform were active in the past with the same configuration. Indeed, to the northeast of the Hillegom transform, the abyssal hills are continuous, curving around the present-day I2 spreading segment (Plate 5). The lack of fracture zone extensions to the active transforms on the ASP Plateau suggests either that the transform faults are not long-lived constituents of the plate boundary (perhaps they evolved recently from nontransform to transform discontinuity) or that volcanism from axis and off-axis sources obscures the transform fabric formed at the plate boundary. In all likelihood, a combination of these sources is responsible and is a consequence of this plate boundary setting near a hotspot.

This rapid evolution is also observed in the behavior of smaller ridge axis discontinuities. Segment J1 is composed of three neovolcanic zones which overlap in an en echelon manner; the overlap of each occurs over a distance equal to about half of its length (Plate 2). The individual segments are >10° oblique to the typical spreading center orientation, and their combined orientation is ~20° oblique to that direction. Steady spreading with this oblique and overlapped plan view geometry is not possible for a significant amount of time, and indeed off-axis V-shaped seafloor features indicate the rapid propagation and realignment of this segment. No typical abyssal hills are formed by J1. While not as clear as J1, the northern short segment of I2 has a similar oblique orientation and less strongly lineated topography (Plate 5).

## 5. Amsterdam-St. Paul Plateau

Typical seafloor depths on the ASP Plateau are 1000-2000 m, ~1 km shallower than young seafloor adjacent to the platform (Plate 2 and Figure 2). The ~400 km along-axis shallow anomaly of the ASP Plateau is superimposed on a longer-wavelength trend of increasing axial depths toward the northwest (Figure 2), noted above and thought to arise from the diminishing influence of the Kerguelen hotspot.

To the north, the ASP Plateau is bounded by the active Amsterdam transform fault and a portion of its inactive fracture zone. This fault forms a nearly 1-km vertical step in the seafloor, across a lateral distance <10 km. To the south, the ASP Plateau boundary is marked by a propagating rift (Plate 2) along segment J2, which is lengthening southward and rifting crust formed ~2 Ma. This propagation has been occurring since at least 1 Ma. The western boundary of the platform occurs a few tens of kilometers to the west of Amsterdam and St. Paul Islands, although it is not well surveyed. From limited crossings, there do not appear to be tectonic features associated with this boundary, and it is likely that the drop off the platform is primarily constructional, with modification by mass wasting. To the east, the boundary of the platform is unsurveyed; part of it abuts the inactive St. Paul fracture zone. To the northeast, the boundary is marked by two troughs in the satellite altimetry (Plate 1) which are possibly remnant spreading centers prior to southward jumps of the SEIR [*Conder et al.*, this issue]. The long dimension of the ASP platform, parallel to the direction of plate spreading, is about 240 km; this represents ~3.5 Myr of spreading at the current SEIR spreading rates. As *Conder et al.* [this issue] infer from magnetic and morphologic studies, however, the spreading on the ASP Plateau has not been continuous, and there is evidence for greater integrated crustal accretion toward the northeast due to southwestward ridge jumps.

At least five patches of seafloor away from the SEIR spreading axis are highly reflective in side scan maps (Figure 1b). With the exception of one small patch near the southeastern end of segment J4 (yellow star in Plate 3b), these reflective areas all occur on the ASP Plateau on the Antarctic plate

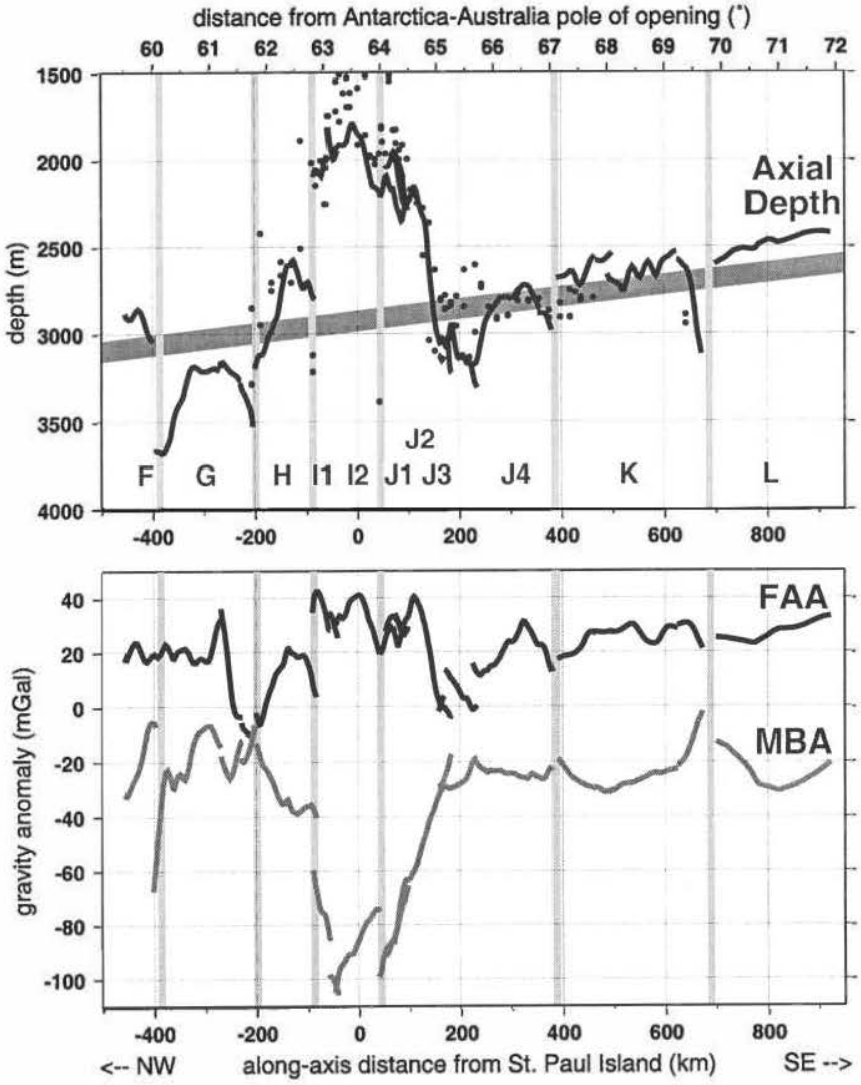


**Figure 2.** Along-axis variations in (top) depth and (bottom) gravity anomalies plotted versus distance from the NUVEL-1A pole of opening (top axis label) and versus the along-axis distance from the point where St. Paul Island intersects the SEIR (bottom axis label). Spreading segments are labeled, and vertical lines indicate the position of the main ridge axis discontinuities. Thick shaded line indicates a regional bathymetric trend of the SEIR, deepening to the northwest. Circles in Figure 2 (top) indicate depths for 1 Ma seafloor. FAA, free-air anomaly; MBA, mantle Bouguer anomaly.

(Plate 5b). A number of these were sampled with dredge and wax core recoveries which all included glassy basalts with little evidence for seafloor weathering or sediment. The side scan amplitudes are comparable to those within ~10 km of the spreading axis on the platform, suggesting that these areas are covered with basalt erupted in the past hundred thousand years, assuming that the lava flow types are similar between the on-axis and off-axis areas. The largest of these reflective areas, >1500 km$^2$, is associated with the shallow Boomerang Seamount (Plate 5b) where there is geochronologic evidence for very recent activity [Johnson et al., submitted manuscript, 1999]. Other off-axis reflective areas are considerably smaller, with lateral dimensions less than several tens of kilometers.

## 6. Axial Morphology Away From the ASP Plateau

Like most intermediate-rate spreading centers elsewhere, the morphology of the SEIR in the study area displays neither the axial high typical of fast spreading center nor the deep valley typical of slower spreading centers. Away from the ASP Plateau the axis of spreading is often within a small valley, 100-500 m deep and 5-15 km across; this valley deepens and widens toward transform faults (e.g., Plate 4a and Figure 3c). The segments closest to the ASP Plateau, G, H, and J3, are characterized by valleys along their entire lengths. These valleys are most obvious in the satellite gravity data (Plate 1), which has a horizontal resolution limit of ~25 km [*Sandwell*

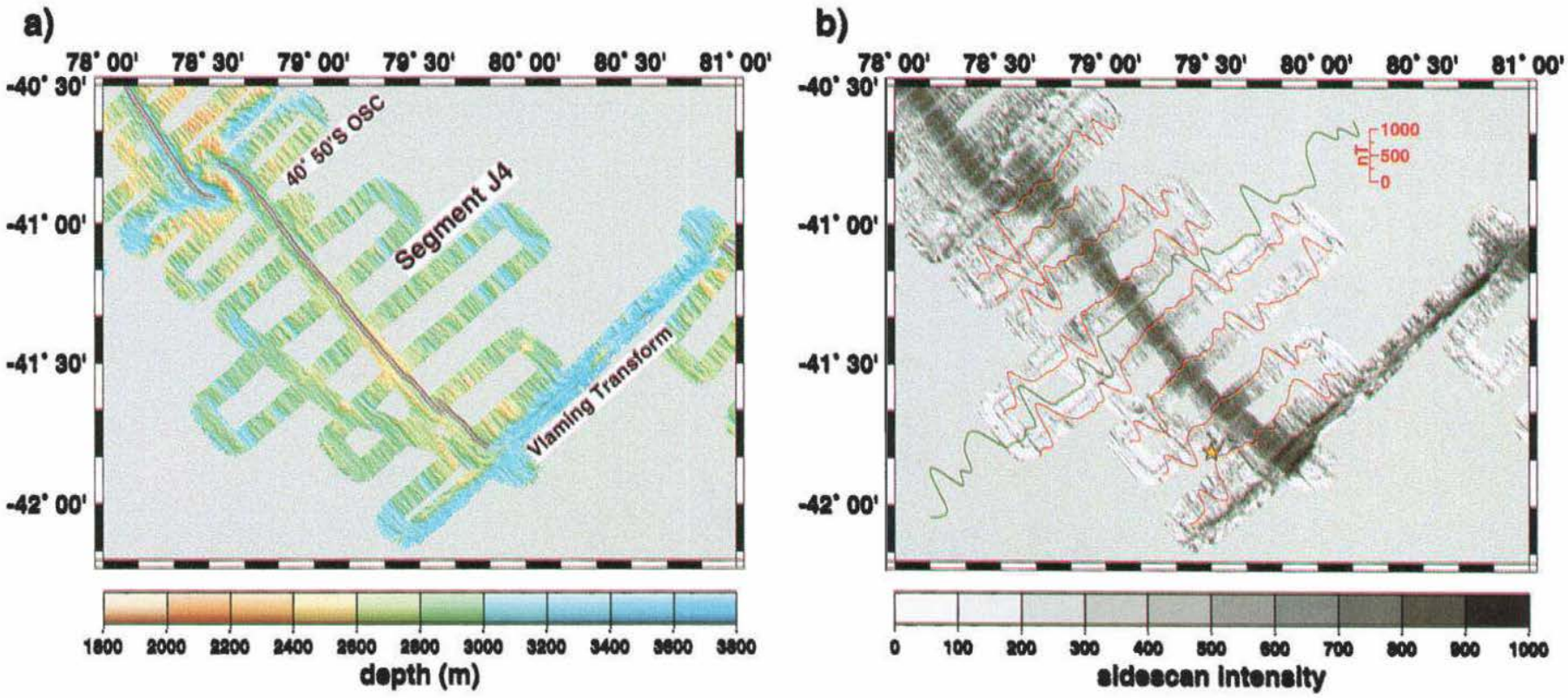


**Plate 3.** (a) Bathymetry and (b) side scan maps of segment J4 to the south of the ASP Plateau. Red wiggles superimposed on the side scan map show the measured magnetic anomalies for selected axis crossings, and the green wiggle shows predicted anomaly from a simple spreading model [*Conder et al.*, this issue]. Yellow star is plotted adjacent to an off-axis patch of high side scan reflectivity.

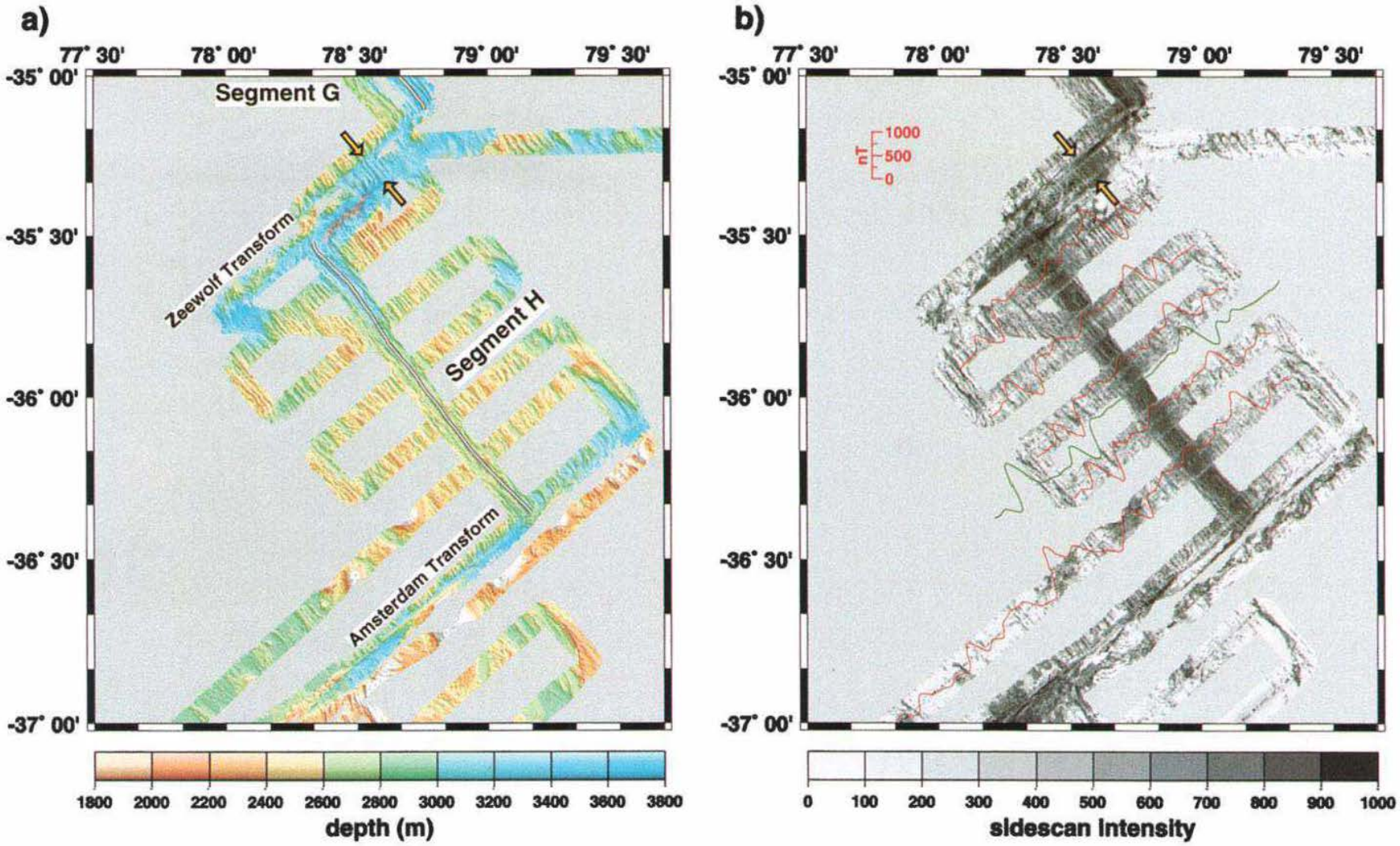


**Plate 4.** (a) Bathymetry and (b) side scan maps of segment H to the north of the ASP Plateau. Magnetic anomalies as in Plate 3. Yellow arrows indicate the location of an intratransform spreading center in the Zeewolf transform fault.

*and Smith*, 1997] and is sensitive to seafloor variations smoothed over that scale. Elsewhere, the spreading axis may be a slight (<500 m), broad high which itself has a <200 m deep central notch (e.g., Plate 3a and Figure 3a). Beyond about 20 km from the axis, the seafloor subsides in response to cooling of the plate.

Lineated abyssal hills form parallel to the spreading center and the magnetic anomalies (Plates 3 and 4). These abyssal hills have relief of 50-250 m and a horizontal separation of 1-3 km (Figure 3). These abyssal hills are similar in dimension to those observed at SEIR segments to the southeast of this study area [*Goff et al.*, 1997]. Isolated, circular seamounts ranging in height from ~200 m (Plate 3a) to ~1200 m obscure the abyssal hills in places (e.g., Plate 4a).

Magnetic anomalies away from the hotspot platform are clear and easy to correlate with the global magnetic reversal sequence (Plates 3 and 4). Spreading asymmetry is generally <10% with no systematic magnitude or sense of asymmetry across the study area. The measured total opening rates vary from 63 km/Myr in segment H to 65 km/Myr on segment K [*Conder et al.*, 1996], values slightly lower than those predicted from the global NUVEL-1A plate motions model [*DeMets et al.*, 1994].

## 7. Axial Morphology on the ASP Plateau

The morphology of the spreading center on the ASP Plateau is also neither a distinctive valley nor an axial high. Topographically, the longer segments on the platform (I2, J2) are situated in broad lows (10-30 km across), and the seafloor does not subside away from the spreading center as expected (Plate 5). The locations of the spreading segments would be difficult to detect from bathymetry alone. The side scan data across the platform delineate the neovolcanic zones associated

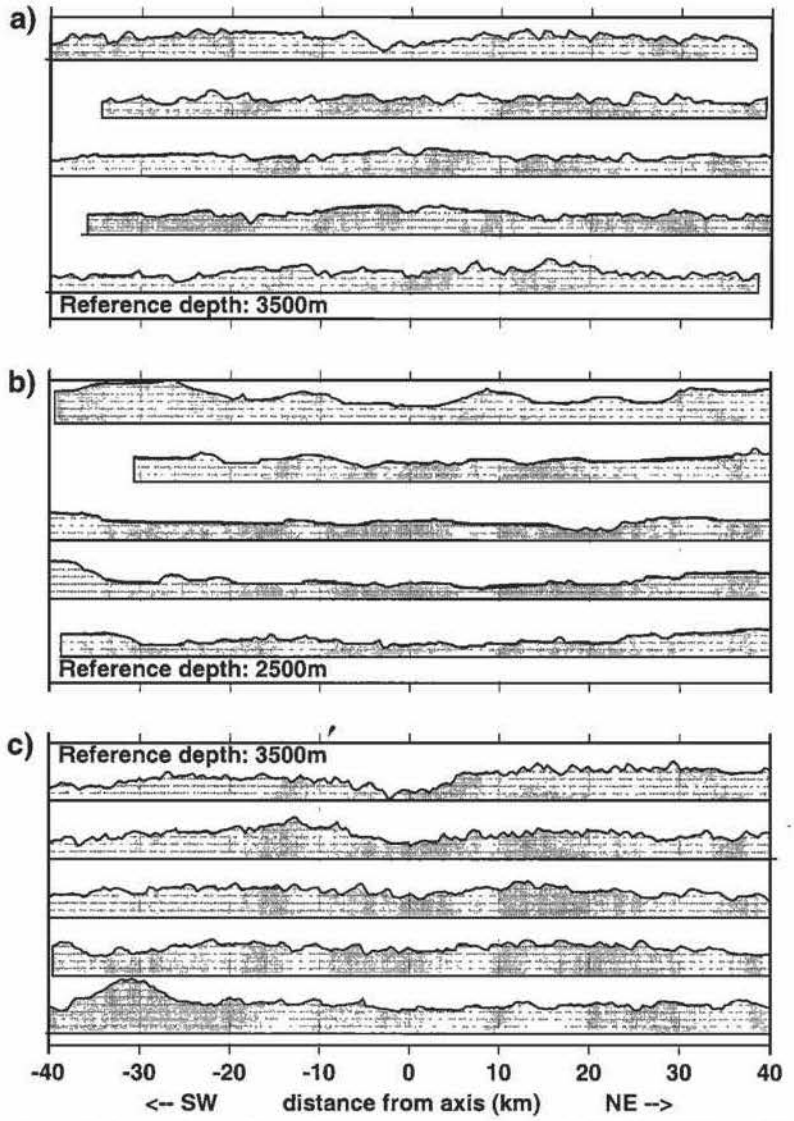


**Figure 3.** Center beam bathymetric profiles of the lines crossing segments (a) J4, (b) I2, and (c) H. The base of the shaded region for each profile is at a depth of 3500 m for the off-platform lines (Figures 3a and 3c) and 2500 m for the on-platform lines (Figure 3b); the horizontal grid lines are spaced at 250 m depth intervals. The vertical exaggeration is 3.3.

with the spreading segments, and the most reflective zones are slightly narrower than those away from the platform (Plate 2). The more rapid near-axis reflectivity decrease on the platform (Plate 2) is probably due to higher sedimentation rates. Also, away from the axial and off-axis neovolcanic zones, the average side scan intensity of the ASP Plateau seafloor is slightly lower than that of the off-platform seafloor (Plate 2). Although we did not collect sediment thickness information, we expect that enhanced biological productivity associated with the shallow plateau, mass wasting from large edifices, and sediment redistribution are responsible for this difference between the on-platform and off-platform seafloor. The calcite compensation depth, >4 km in this area [*Kennett*, 1982], is probably not a factor in governing the sediment accumulation patterns in these near-axis regions.

Abyssal hills are smaller and less continuous on the platform than elsewhere (Figure 3b). This cannot be explained solely by the masking effects of thicker sediments, given that many isolated, 50 m and taller features are evident. More likely, the formation of smaller and less regular abyssal hills, combined with the potential of fault scarp burial from off-axis volcanism, explains this difference in seafloor fabric. As noted above, the abyssal hills which are present often curve near the ends of spreading segments, sometimes extending beyond the segment tips.

## 8. Gravity Analysis and Inferred Structure at Depth

The shipboard free-air gravity anomalies were interpolated onto a 1 km grid (Plate 6a) using the projection onto convex sets (POCS) interpolation method [cf. *Conder et al.*, this issue]. The shipboard anomalies are more detailed than their satellite counterparts (Plate 1), and they mimic the short-wavelength topography (Plate 2a) of seamounts, transform fault valleys, and axial depressions. At longer wavelength (>40 km), the free-air anomaly variation does not mimic the topographic variation as closely, and the broad ASP Plateau topographic anomaly is muted in the free-air data (Figure 2 and Plate 6). This low correlation of free-air anomaly and longer-wavelength topography is common in oceanic settings, indicating the isostatic compensation of broad topographic features at depth.

Because the gravitational effect of the seafloor variation is well-known and because it contributes a large component to the measured sea-surface gravity, we remove the effect of the seafloor from the shipboard anomalies to infer deeper lateral density variations. Following the now standard method of *Kuo and Forsyth* [1988], we calculate the gravitational effects of a 1.7 g/cm$^3$ density contrast at the seafloor, a 0.2 g/cm$^3$ density contrast at a depth 2 km below the seafloor, and a 0.4 g/cm$^3$ density contrast at the Moho (here assumed to be 6 km below the seafloor). The gravity predictions from this simple, constant crustal thickness and density-structure model are then removed from the free-air anomalies to produce the mantle Bouguer anomaly (MBA). MBA variations indicate deviations in the actual crustal and mantle structure from this very simple model; negative MBA values indicate mass deficits relative to the model (as would arise from thicker crust or lower density crust and mantle), and positive values indicate mass excesses.

Large negative MBA values are associated with the ASP platform (Plate 6b), and the most negative anomalies coincide with the shallowest seafloor. The along-axis variation in MBA is presented in Figure 2. The implied mass deficit is strong evidence for local compensation of the platform features at depth, either by crustal thickening, lower densities in the crust, lower mantle densities, or a combination of these factors.

Away from the ASP Plateau, MBA values increase with distance from the spreading axis, an effect of lithospheric cooling as the crust and mantle become older and denser [e.g., *Kuo and Forsyth*, 1988]. Similar to spreading centers elsewhere, the MBA contours along segments J4 and K close toward axial discontinuities, diagnostic of along-axis reductions in temperature and/or inferred crustal thickness toward these ridge offsets.

In contrast to the FAA behavior, the MBA contours are not simply correlated with the spreading segment geometry on the ASP Plateau (Plate 6b). Segments I1, J1, and J2 cut across the MBA gradients. Segment I2 parallels the MBA contours for the most part, but rather than being situated in an MBA low (as for the off-platform SEIR segments and many spreading centers elsewhere), I2 coincides with a local MBA high. These complexities in the MBA for the on-platform segments are indicative of a rapidly evolving plate boundary, extensive off-axis volcanism, and temporal variations in crustal production at the spreading center. The decrease in MBA perpendicular to segment I2 corresponds to the absence of seafloor subsidence, noted above, and may be a result of declining crustal production as the ridge begins to migrate away (to the NE) from the hotspot now located beneath the Antarctic plate.

On segment H, immediately to the north of the ASP Plateau, the MBA has the expected increase with crustal age. The MBA contours close, as expected, approaching the Zeewolf transform to the north. However, to the south near the Amsterdam transform, the MBA retains a low value. This indicates that the crustal thickening and/or thermal effects of the ASP Plateau extend at least partway along segment H, significantly to the north of the topographic platform anomaly. This is consistent with evidence from helium isotopes which indicate an extension of the mantle plume geochemical anomaly to the northwestern end of segment H but not across the Zeewolf transform to segment G [*Graham et al.*, 1999].

Marine gravity analysis often proceeds to calculate a residual MBA to account for the thermal aging effects on gravity. These residual anomalies are often used to assess the importance of lateral density variations which might occur from thickness or compositional (density) variations of crustal units or temperature. In most studies of gravity alone, discriminating among these possible causes is impossible. For the ASP Plateau data set, residual MBA's were calculated, but they are not useful for two reasons: the present-day plate boundary is more complex, with curving and overlapping segments, than this simple model can account for and the boundary has evolved significantly over timescales of <1 Myr.

Nonetheless, some inferences about deeper structure can be made simply from the MBA map (Plate 6b). The greatest MBA variation is closely associated with the ASP Plateau topography. If we make the assumption that the topography of the platform is isostatically compensated in a local (Airy)

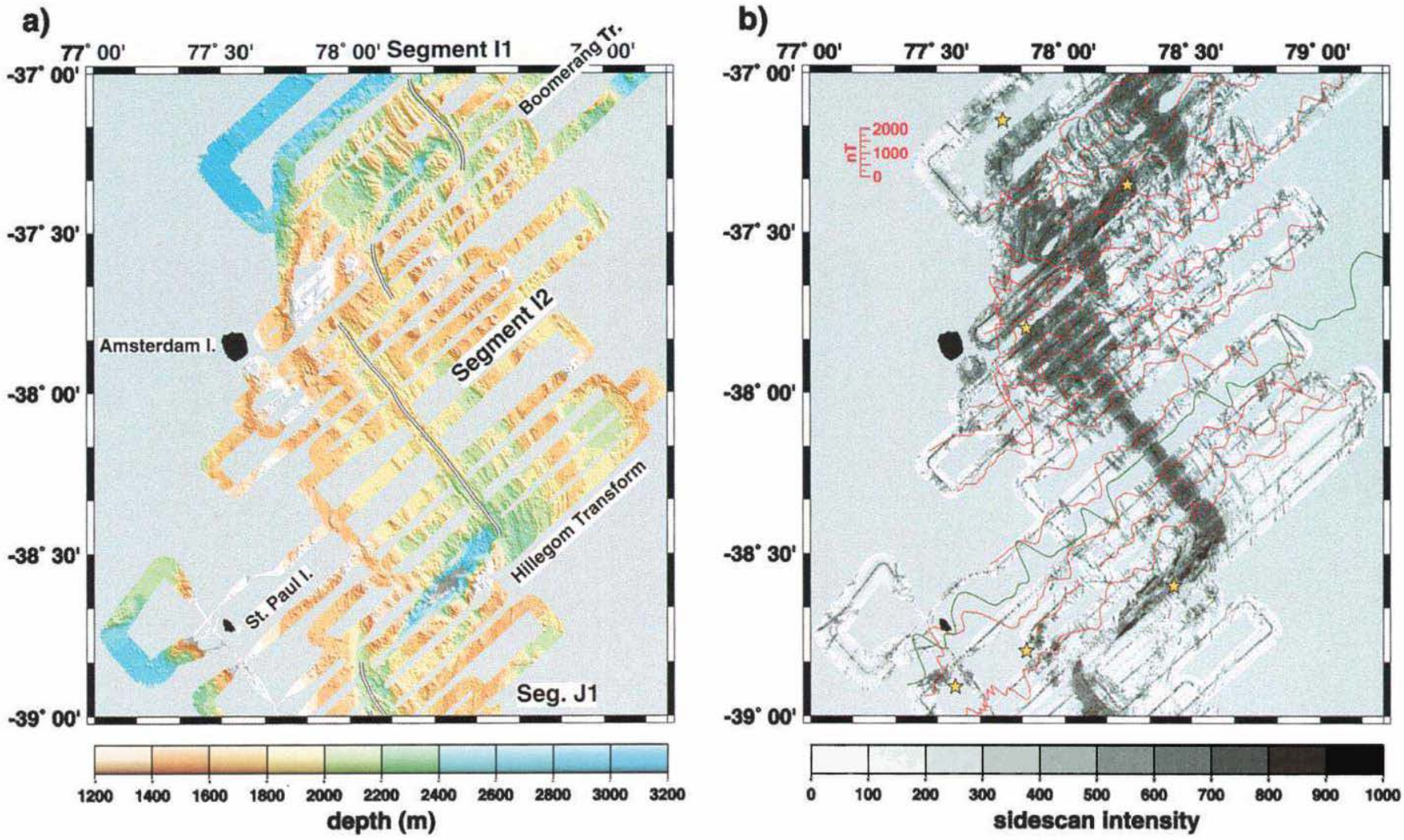


**Plate 5.** (a) Bathymetry and (b) side scan maps of segments I1 (at top) and I2, which cross the ASP Plateau. Yellow stars and magnetic anomalies as in Plate 3, although the wiggle scale is compressed by a factor of 2 to account for the larger anomalies associated with the shallower seafloor depths.

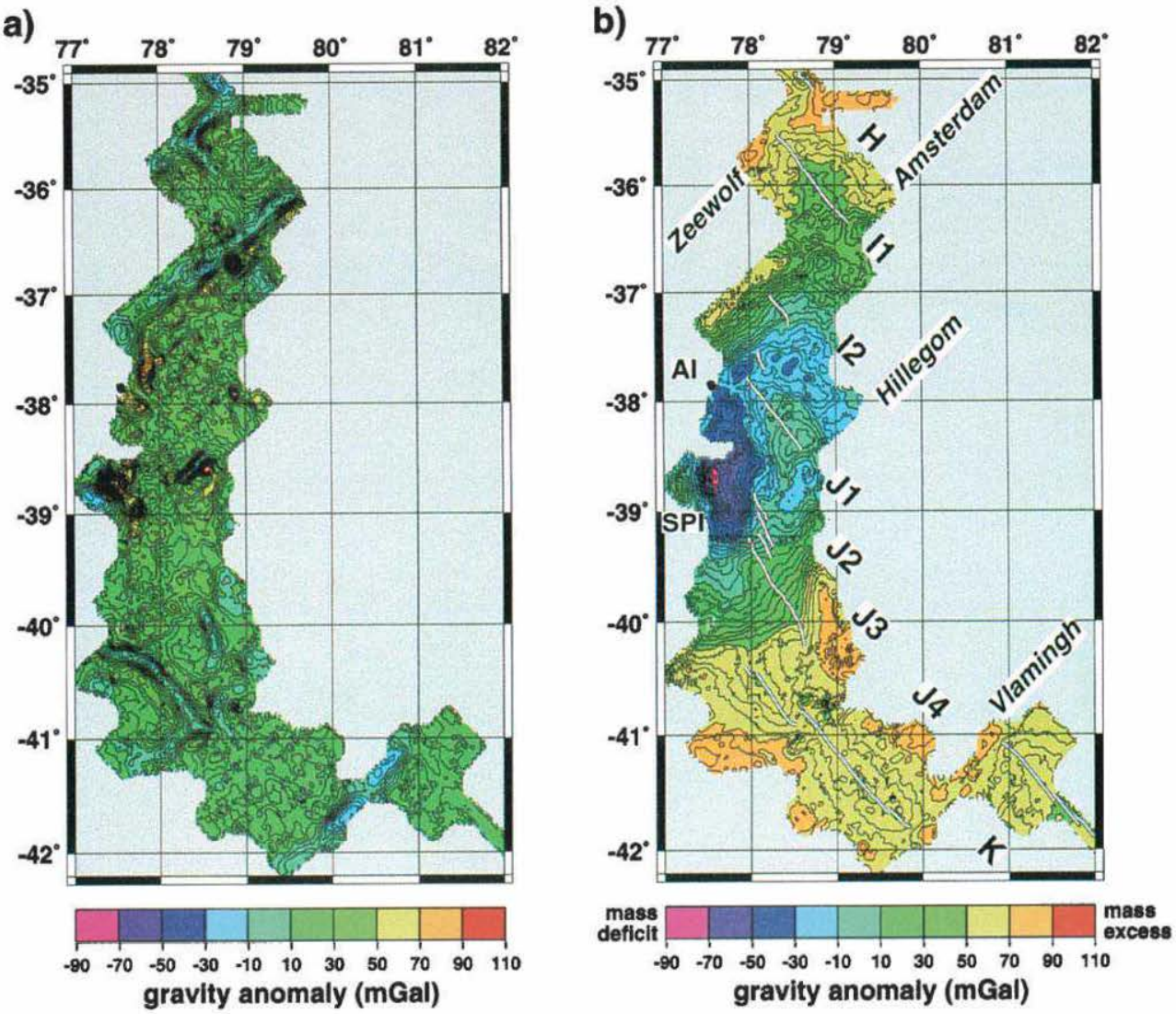


**Plate 6.** (a) Gridded shipboard free-air anomalies and (b) mantle Bouguer anomalies for the area displayed in Plate 2. In both cases the fields have been interpolated with a POCS interpolator and are contoured at 5 mGal.

manner or with a very weak flexural plate, then we can use both the topographic and MBA variation to infer the depth at which compensation is occurring. This assumption of local isostasy may be nearly correct because there is only a very small free-air anomaly associated with the ASP Plateau (Plate 6a) and there are no identifiable flexural moats surrounding the large, on-platform volcanic edifices (see discussion of flexural rigidity, below). We identify seafloor shallower than 2800 m as representing the anomalous topography of the platform (Figure 4a). Then we consider three simple models of local compensation which could support this topography: crustal thickness variation, mantle which is 200°C hotter beneath the platform than elsewhere, and 50°C hotter mantle beneath the platform. A 200°C temperature anomaly is at the large limit of anomalies inferred from hotspots elsewhere [*Sleep*, 1990; *Schilling*, 1991]. Figure 4b illustrates cross sections through these models; local compensation models simply reflect the topographic variation into the compensating surfaces. In the crustal compensation model a crustal root of 5-8 km thickness supports the main part of the platform; beneath the shallowest topography, the crustal root would be twice that thickness. In the 200°C hotter mantle compensation case the hot mantle root would extend to depths of 80-150 km; in the 50°C hotter mantle case the hot mantle root would extend to 300-400 km, on average.

While each of these simple compensating models would support the anomalous platform topography equally well, they have very different gravitational predictions because of the different depth extents of the compensating surfaces. Figure 5 illustrates the predicted gravity anomalies for these three models in comparison to the MBA. Clearly, the compensating root must be relatively shallow, and the Moho source best matches the MBA amplitude and pattern. However, the fact that the shortest-wavelength signal of the MBA is not predicted in the crustal compensation model indicates that some of the isostatic compensation occurs at depths shallower than the Moho or that compensation is not complete, perhaps due to lateral variations in crustal lithology, temperature, or constituent layer thickness which are not correlated with surface topography. Some of the platform's compensation may be explained by hotter temperatures in the mantle, but these deeper contributions are necessarily small and not well-resolved by the gravity analysis (cf. the lack of detail in the 200°C and 50°C panels of Figure 5).

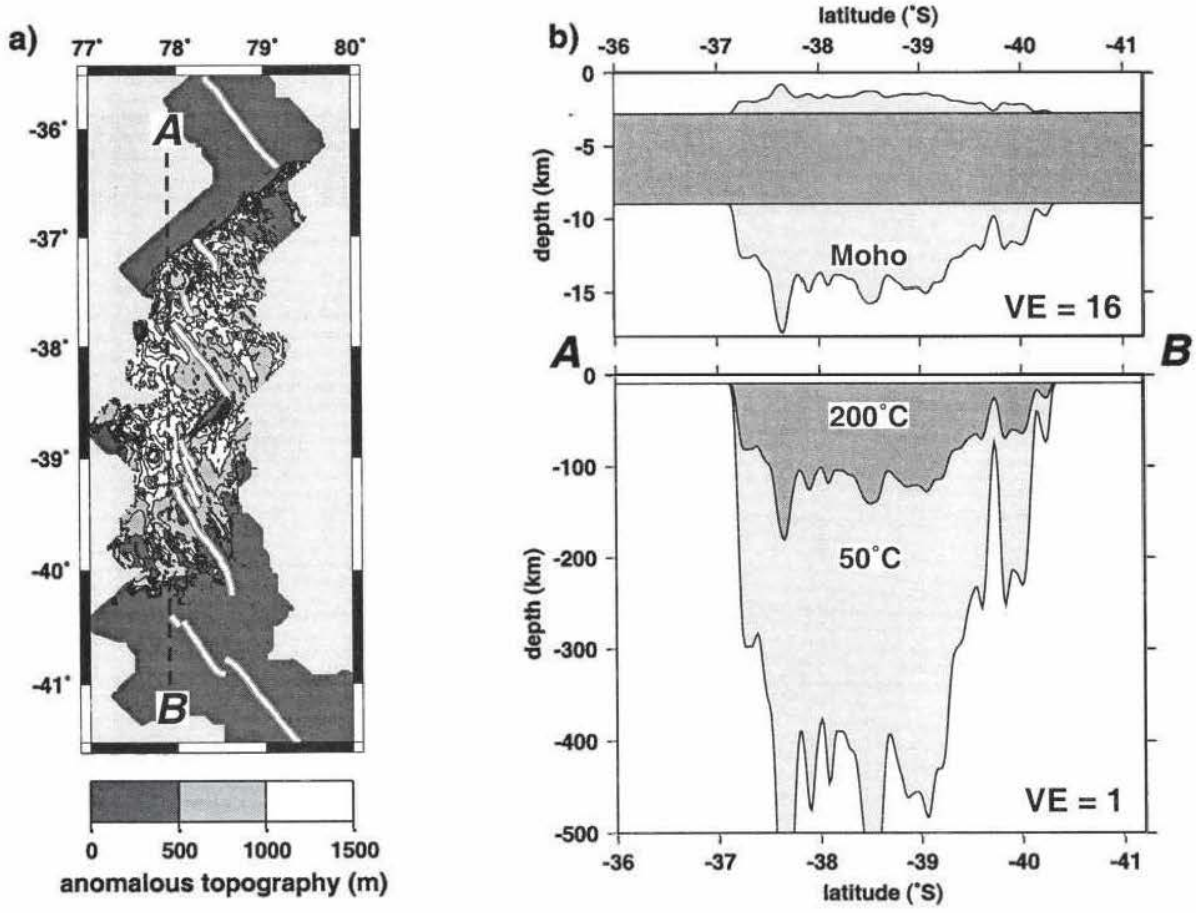


**Figure 4.** (a) Anomalous topography of the ASP platform, defined as the seafloor elevation above the 2800 m depth level. Contours are every 500 m. Dashed line indicates the profile A-B, shown in Figure 4b. (b) Cross sections of the anomalous topography (topmost profile) and surfaces at depth which would compensate this topography locally. "Moho" region delineates a crustal root if the compensation is due solely to Moho depth variations. The "200°C" area indicates the region of compensating mantle required if it is uniformly 200°C hotter than surrounding mantle. Likewise, "50°C" indicates the larger mantle region required with a temperature anomaly of 50°C.

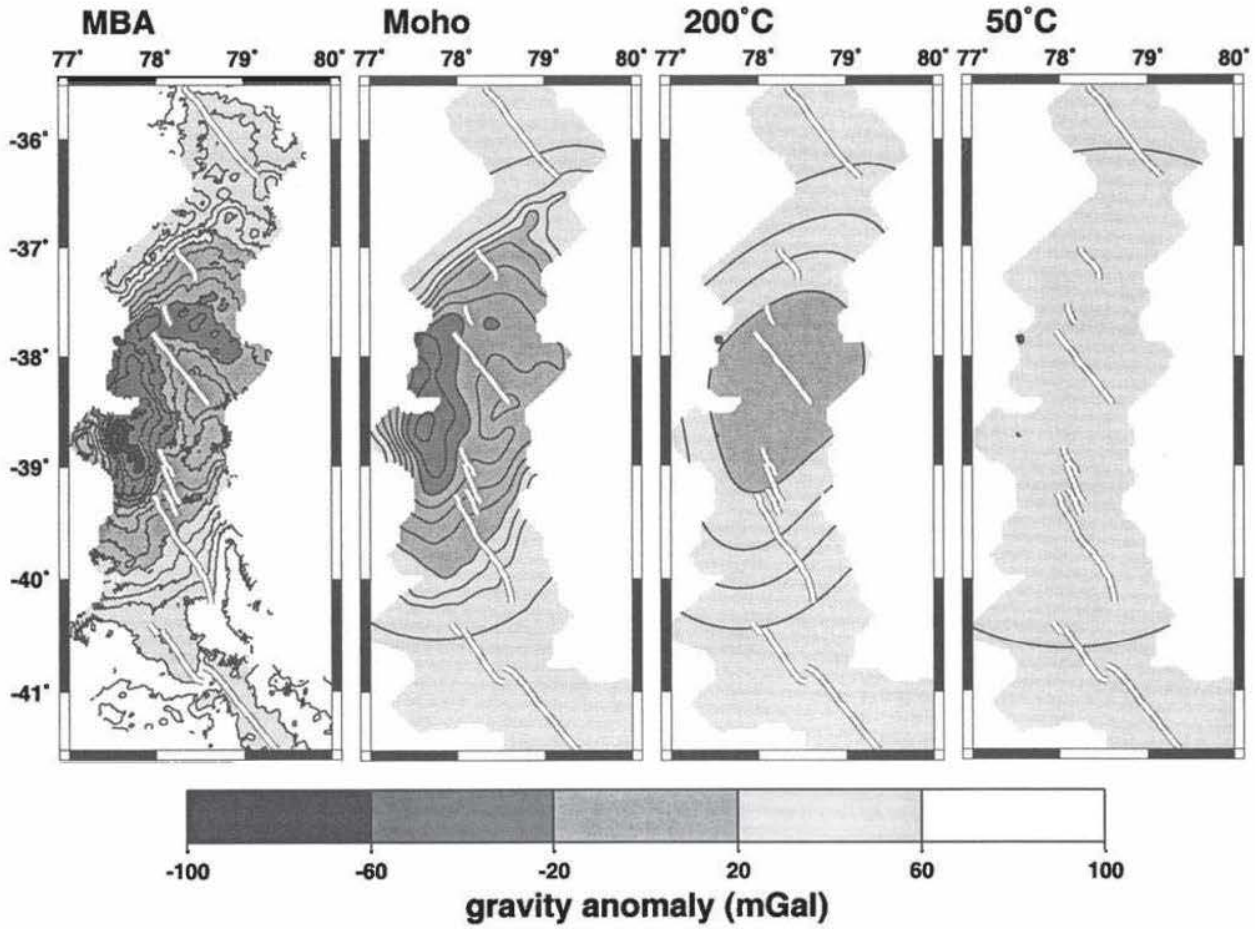


**Figure 5.** (left) Observed mantle Bouguer anomaly and model gravity anomalies assuming local compensation due to the models in Figure 5. Gravity anomalies are contoured at 10 mGal, and their base values away from the ASP Plateau have been set to the same value to aid in comparisons.

The compensation of topography can also be constrained in the spectral domain using coherence and admittance analysis of gravity anomaly (a proxy for the compensating density surface at depth) and bathymetry [e.g., *Forsyth*, 1985; *Blackman and Forsyth*, 1991; *Neumann and Forsyth*, 1993]. Assuming that preflexure loads at depth are uncorrelated with preflexure loads at the seafloor, theoretical coherence and admittance spectra for the flexed configuration may be calculated for a variety of plate rigidities (or, equivalently, effective elastic thicknesses $T_e$), average compensation depths, and proportions of top and bottom loading. These theoretical curves may then be compared with coherence and admittance spectra derived from gravity anomaly and bathymetry data, in this instance, in gridded form. The transition from high coherence between MBA and bathymetry at long wavelengths to low coherence at short wavelengths is a sensitive indicator of the plate thickness supporting isostatic loads [*Forsyth*, 1985]. Given a plate thickness estimated from coherence, the depth of compensation and proportion of bottom loading may then be estimated from the admittance spectrum.

For this analysis, a complete (or crustal) Bouguer anomaly (CBA) is used as the gravity anomaly because it is more representative of the compensating surface than the MBA, which assumes a form for the Moho variation. The CBA is calculated simply by subtracting the gravitational effects of the seafloor (1.7 g/cm$^3$) and intracrustal (0.2 g/cm$^3$) density contrasts from the FAA. Coherence and admittance spectra for the SEIR are presented in Figure 6. The spectral calculations are performed on the gridded data, but the resulting 2-D spectra are averaged in wavenumber bins for comparison with models which assume isotropic response functions [e.g., *Blackman and Forsyth*, 1991; *Neumann and Forsyth*, 1993]. Spectra from a single area encompassing the top of the surveyed platform are presented in Figure 6a, and the combined spectra of three areas off the platform (segments H, J3, and J4) are presented in Figure 6b. The clear difference between the coherence spectra is the transition wavelengths from high to low coherence; on the ASP platform this occurs at wavelengths of 30-60 km, and off the platform it occurs at 60-140 km. These coherence transitions may be explained by $T_e$ of 1.6 and 4 km (Figure 6), respectively, corresponding to a more than 15-fold increase in flexural rigidity from the platform to the adjacent segments. While formal estimates of the standard error of $T_e$ are typically 10-15%, a more conservative estimate is that variations in $T_e$ of a factor of 2 can be resolved with confidence [*Bechtel et al.*, 1990]. The 4-km effective elastic thickness for the off-platform segments is similar to values obtained for portions of the slow spreading Mid-Atlantic Ridge [*Blackman and Forsyth*, 1991; *Neumann and Forsyth*, 1993]; the 1.6-km thickness for the elastic plate beneath the ASP Plateau confirms the very

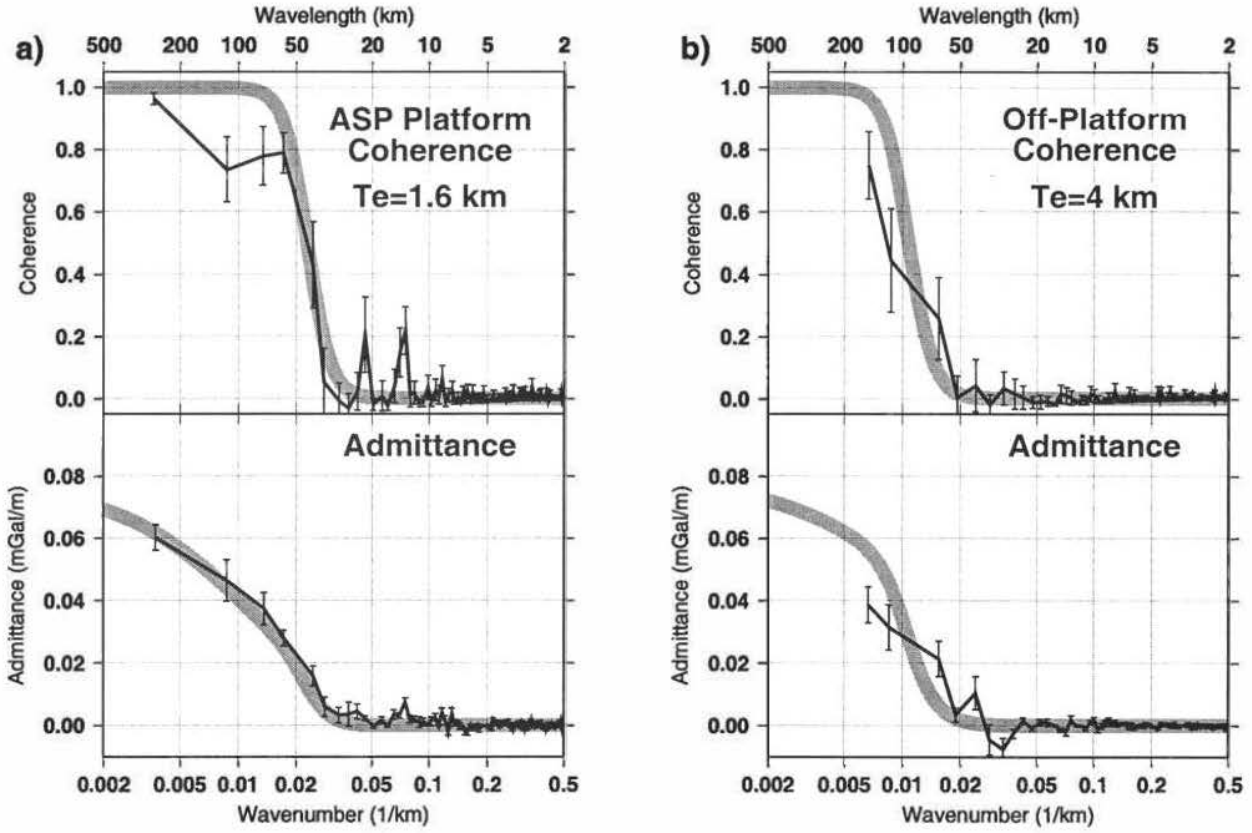


**Figure 6.** Coherence and admittance spectra of complete Bouguer anomaly and bathymetry (a) for the surveyed portion of the ASP Plateau and (b) for three areas off the platform. The shaded lines illustrate theoretical coherence and admittance spectra assuming the isostatic parameters described in the text.

weak nature of the plate there, bringing about essentially local compensation of the platform topography. The measured spectra differ from the theoretical curves in several ways: long-wavelength coherence values do not reach 1.0, the ASP coherence transition is broader than that of any theoretical model, and there are some significantly nonzero coherence estimates at wavelengths shorter than the transition. These differences have been observed in other studies, and they are likely a result of lateral variation in compensation parameters within the study regions and of the limited sizes of these regions.

The admittance spectrum for the platform is adequately fit using an average compensation depth of 11 km below sea level and bottom loading equal to 75% of the top loading. The off-platform admittance can be explained with an average compensation depth of 8 km below sea level and a bottom loading fraction of 50%. These parameters are not as well constrained as $T_e$, however, because spectral estimates are sparse for wavelengths >100 km and because there is a trade-off between the compensation depth and the fractional loading value. Indeed, it is unlikely that the depths of compensation and fractional loading parameters are constant across all of the wavelengths, so the values chosen to generate the synthetic curves in Figure 6 are best used for illustration. Like the effective elastic thickness, the depth of compensation derived from this analysis is only a single representative value which falls within the range of actual compensation depths. Nonetheless, an average compensation depth of 11 km below sea level for the ASP Plateau and the average seafloor depth of 1-2 km imply that isostatic compensation occurs at an average depth of 9-10 km below the seafloor on the platform, i.e., within the lower crust and at the Moho of thickened oceanic crust. The average compensation depth of 8 km below sea level for the off-platform crust, along with the average ~3 km seafloor depth of these segments, implies that the compensation occurs about 5 km below the seafloor, in the lower crust and at the Moho of normal thickness oceanic crust. The proportions of lithospheric loading from the bottom relative to the top which are consistent with the observed admittance spectra range between 10% and 100%. Although not well-constrained by this analysis, these values suggest that significant underplating of low-density material occurs at the base of the crust and within its lower levels. Lateral variations in the density of crustal units, such as the likely thickening of a low-density volcanic layer beneath a seamount edifice, introduce a contribution of Pratt isostasy to the Airy-type isostasy inferred from compensation at the Moho.

## 9. Discussion

The enhanced volcanic activity on the ASP Plateau influences all of the geophysical and tectonic characteristics of young seafloor relative to its counterpart away from the platform or at other intermediate-rate spreading centers. Recent volcanism on the platform occurs in two distinct settings: centered on the SEIR spreading segments and in isolated patches off-axis on the Antarctic plate. This distribution of off-axis

volcanism, the presence of the two islands and other shallow edifices on the Antarctic plate, and the motion of the tectonic plates over the hotspot frame of reference indicate that ASP hotspot activity is currently situated beneath the Antarctic plate but very near the SEIR (<100 km). Johnson et al. [submitted manuscript, 1999] present evidence that the Boomerang Seamount, only 25 km southwest of the nearest SEIR spreading segment, erupted as recently as December 1995. Thus, if one were to define the ASP hotspot at a single location, it would be beneath the Boomerang Seamount. However, the considerably broader horizontal scale (150-200 km) of the ASP Plateau and the presence of multiple off-axis recent volcanic fields suggest that the surface expression of hotspot volcanism is more extensive. Relative to the smaller, isolated volcanoes of the hotspot trace on the Australian plate, a broader expression of volcanism forming the platform is fostered by the presence of young, weak lithosphere near the spreading center and possible along-axis channeling.

In addition to causing off-axis volcanism, the ASP hotspot also enhances the volcanic production at the spreading center itself, as indicated by the shallow axial depths and the negative MBAs of the platform spreading centers relative to their off-platform counterparts. The smaller abyssal hills observed on the platform suggest that less of the plate separation is accommodated by tectonic extension and more is accommodated by magmatic accretion and also that volcanism may obscure tectonic fabric formed at the plate boundary. Analysis of SEIR MORB compositions demonstrates the strong interaction between magmas from the ASP plume source and a more typical, depleted mantle source [*Johnson et al.*, 1996; *Douglas Priebe*, 1998; *Graham et al.*, 1999]. The typical 1-1.5 km shallower depth of the SEIR crossing the platform relative to the spreading segments off the platform suggests production of oceanic crust nearly twice as thick as the 6-7 km thickness observed elsewhere. Away from the spreading center, off-axis magmatism builds volcanic edifices 1000-1500 m shallower than the spreading center. Given the local isostasy which supports these edifices (inferred from forward modeling and spectral gravity analysis), the crust at these sites is thickened by an additional 4-6 km. *Ito and Lin* [1995] observe topographic and residual gravity anomalies associated with the Galapagos hotspot which are similar in magnitude to those of Amsterdam-St. Paul. The lateral extent of the Galapagos anomalies is ~3 times greater than ASP, however. *Ito and Lin* [1995] attribute ~70-75% of the isostatic compensation to be due to crustal thickness variations; the remainder is attributed to mantle density variations arising from temperature anomalies of 50-90°C beneath the hotspot. Near ASP, such temperature anomalies are difficult to distinguish in the geophysical data; clearly they cannot be the sole support for the platform topography (Figure 5), and small temperature anomalies in the upper mantle produce low-amplitude gravity anomalies with a lateral extent which is large relative to the size of the survey area.

Beyond the striking differences of the crustal accretion on and off the ASP hotspot platform, other effects of the hotspot appear to be present in the spreading segments adjacent to the hotspot platform. The most significant axial valleys in the study area occur in segments G, H, and J3 (Plate 1), adjacent to the ASP Plateau. Segments G and J3 also form local depth maxima in the along-axis profile of the SEIR (Plate 4), 300-500 m deeper than the adjacent segments farther from the platform. The spreading rate variation among these segments is negligible, so other causes must govern these depth differences. Some of this difference is due to the presence of uncompensated axial valleys at these segments. The axial morphology of intermediate-rate spreading centers is very sensitive to differences in axial thermal structure, with valleys indicative of colder, stronger lithosphere [e.g., *Small and Sandwell*, 1989; *Phipps Morgan and Chen*, 1993]. If this is the case for the SEIR, why would such conditions occur immediately adjacent to the ASP hotspot platform?

One possibility is that there is a component of along-axis mantle flow away from the hotspot, as inferred independently from helium isotope analysis of the seafloor basalts [*Graham et al.*, 1999]. Mantle that originally wells up and melts partially beneath the platform and then migrates laterally away from the platform would inhibit melting beneath the adjacent segments; less mantle upwelling from depth beneath these segments would be required to accommodate the plate spreading and lateral input of partially depleted and cooler mantle would hinder melting. Reduced melting would diminish the likelihood of a long-term crustal magma chamber and result in stronger lithosphere to produce a well-defined axial valley and deeper spreading center. The merging of the MBA contours of segments H and J3 with the MBA low of the ASP Plateau (Plate 6b) indicates that the hotspot platform structure at depth extends beyond the topographic boundary of the platform itself. Independent evidence for the extension of the hotspot influence to segments away from the platform comes from geochemical analyses of the major and trace elements and helium isotopic compositions of the lavas, especially along segment H [*Johnson et al.*, 1996; *Graham et al.*, 1999]. Segment H exhibits some of the largest hotspot geochemical anomalies of any of the studied segments, and it also is characterized by the most diverse lava compositions of any of the segments. On the basis of these observations, *Graham et al.* [1999] suggest that the mantle beneath segment H derives from the outer portions of the ASP plume.

Thus, even though the ASP hotspot is small in comparison to other hotspots, it fundamentally alters the way in which oceanic crust is created at the SEIR. Crustal accretion occurs at a rapidly evolving plate boundary, more than twice as much crust is produced than elsewhere, off-axis volcanism is widespread, abyssal hill creation is diminished, and geochemical anomalies are present in the erupted basalts. Even away from the topographic platform marking the locus of hotspot volcanism, seafloor spreading is affected by along-axis mantle flow which alters the thermal conditions at segments as much as 50-200 km away from the topographic platform boundaries. The setting of this portion of the SEIR, very near to the low-flux ASP hotspot and far from the high-flux Kerguelen hotspot, presents an unusual opportunity to study a variety of ridge-hotspot interactions and their superposition. While the Kerguelen hotspot influence is largely evident in long-wavelength topographic and morphologic trends of the SEIR, the ASP hotspot creates variability of the seafloor depth and plate boundary geometry over much shorter distance scales (tens of kilometers) and time durations (<1 Myr).

**Acknowledgments.** We thank the R/V *Melville's* officers and crew and the Scripps Shipboard Technical Support staff for the success of Boomerang, Leg 6. We thank the French government agency, Territoire des Terres Australes et Antarctiques Françaises, for permission to work in their territorial waters. Base maps for cruise planning were provided by M. Munschy and R.L. Fisher. The satellite

gravity anomaly data provided by *Sandwell and Smith* [1997] were an indispensable aid to surveying this remote spreading center. We are grateful to David Caress for providing the software to process the SeaBeam2000 side scan data at full dynamic range. The MB System [*Caress and Chayes*, 1996] and GMT [*Wessel and Smith*, 1995] software packages were used extensively in this study. We appreciate the reviews of Neil Mitchell, Donna Blackman, an anonymous reviewer, and the Associate Editor. This work is supported by NSF grant OCE-9505667 of the RIDGE Initiative.

## References

Bechtel, T D., D. W. Forsyth, V. L. Sharpton, and R. A. F Grieve, Variations in effective elastic thickness of the North American lithosphere, *Nature, 343,* 636-638, 1990.

Blackman, D. K , and D. W. Forsyth, Isostatic compensation of tectonic features of the Mid-Atlantic Ridge: 25-27°30'S, *J Geophys. Res , 96,* 11,741-11,758, 1991.

Caress, D. W., and D. N. Chayes, Improved processing of Hydrosweep DS multibeam data from the R/V *Maurice Ewing, Mar. Geophys. Res., 18,* 631-650, 1996.

Cochran, J. R., J.-C. Sempere, and the SEIR Scientific Team, The Southeast Indian Ridge between 88°E and 118°E Gravity anomalies and crustal accretion at intermediate spreading rates, *J. Geophys Res., 102,* 15,463-15,487, 1997.

Conder, J. A., D. S. Scheirer, and D. W. Forsyth, Magnetic anomalies of the Southeast Indian Ridge near the Amsterdam-St. Paul platform, *Eos Trans. AGU, 77* (46), Fall Meet. Suppl., F684, 1996.

Conder, J. A., D. S Scheirer, and D. W. Forsyth, Seafloor spreading on the Amsterdam-St. Paul hotspot plateau, *J. Geophys. Res.*, this issue.

DeMets, C., R. G. Gordon, D. F. Argus, and S. Stein, Effect of recent revisions to the geomagnetic reversal time scale on estimates of current plate motions, *Geophys. Res. Lett., 21,* 2191-2194, 1994.

Dosso, L., H. Bougault, P. Beuzart, J.-Y. Calvez, and J.-L. Joron, The geochemical structure of the South-East Indian Ridge, *Earth Planet. Sci. Lett., 88,* 47-59, 1988.

Douglas, L. M., D. W Graham, K. T. M. Johnson, D. S. Scheirer, and D. W. Forsyth, Variations in major element composition of basalt glasses along the Southeast Indian Ridge in the vicinity of the Amsterdam-Saint Paul Platform, *Eos Trans. AGU, 77* (46), Fall Meet. Suppl., F690, 1996.

Douglas Priebe, L M., Geochemical and petrogenetic effects of the interaction of the Southeast Indian Ridge and the Amsterdam-St. Paul hotspot, M. S. thesis, Oreg. State Univ., Corvallis, 1998.

Dziewonski, A. M., G. Ekstrom, J. H Woodhouse, and G. Zwart, Centroid-moment tensor solutions for January-March, 1990, *Phys. Earth Planet. Inter., 65,* 197-206, 1991.

Feighner, M. A., and M. A. Richards, The fluid dynamics of plume-ridge and plume-plate interactions: An experimental investigation, *Earth Planet. Sci. Lett., 129,* 171-182, 1995.

Forsyth, D. W., Subsurface loading and estimates of the flexural rigidity of continental lithosphere, *J. Geophys. Res., 90,* 12,623-12,632, 1985.

Goff, J. A., Y. Ma, A. Shah, J. R. Cochran, and J.-C. Sempere, Stochastic analysis of seafloor morphology on the flanks of the Southeast Indian Ridge: The influences of ridge morphology on the formation of abyssal hills, *J. Geophys. Res., 102,* 15,521-15,534, 1997.

Graham, D. W., K. T. M. Johnson, L. Douglas Priebe, and J. E. Lupton, Hotspot-ridge interaction along the Southeast Indian Ridge near Amsterdam and St. Paul Islands· Helium isotope evidence, *Earth Planet. Sci. Lett., 167,* 297-310, 1999.

Gripp, A. E., and R. G. Gordon, Current plate velocities relative to the hotspots incorporating the NUVEL-1 plate motion model, *Geophys. Res. Lett., 17,* 1109-1112, 1990.

Hamelin, B., B. Dupre, and C. J. Allegre, Pb-Sr-Nd isotopic data of Indian Ocean ridges: New evidence of large-scale mapping of mantle heterogeneities, *Earth Planet. Sci. Lett., 76,* 288-298, 1986.

Hitchman, A. P , F. E. M. Lilley, and W. H. Campbell, The quiet daily variation in the total magnetic field: Global fields, *Geophys. Res. Lett., 25,* 2007-2010, 1998.

Ito, G. T., and J. Lin, Mantle temperature anomalies along the present and paleoaxes of the Galapagos spreading center as inferred from gravity analyses, *J. Geophys. Res., 100,* 3733-3745, 1995.

Ito, G., J. Lin, and C. W. Gable, Dynamics of mantle flow and melting at a ridge-centered hotspot: Iceland and the Mid-Atlantic Ridge, *Earth Planet. Sci. Lett., 144,* 53-74, 1996.

Ito, G., J. Lin, and C. W. Gable, Interaction of mantle plumes and migrating mid-ocean ridges: Implications for the Galapagos plume-ridge system, *J. Geophys. Res., 102,* 15,403-15,417, 1997.

Ito, G., Y. Shen, G. Hirth, and C J. Wolfe, Mantle flow, melting, and dehydration of the Iceland mantle plume, *Earth Planet. Sci. Lett., 165,* 81-96, 1999.

Johnson, K. T. M., L. M. Douglas, D. W. Graham, D. S. Scheirer, and D. W. Forsyth, Ridge-hotspot interaction on the Southeast Indian Ridge near the Amsterdam-St. Paul Platform, *Eos Trans. AGU, 77* (46), Fall Meet. Suppl., F684, 1996

Kennett, J. P , *Marine Geology*, 813 pp., Prentice-Hall, Englewood Cliffs, N J., 1982.

Kincaid, C , G. Ito, and C. Gable, Laboratory investigation of the interaction of off-axis mantle plumes and spreading centers, *Nature, 376,* 758-761, 1995.

Kuo, B.-Y., and D. W. Forsyth, Gravity anomalies of the ridge-transform system in the South Atlantic between 31 and 34.5°S: Upwelling centers and variations in crustal thickness, *Mar. Geophys. Res., 10,* 205-232, 1988.

Ma, Y., and J. R. Cochran, Transitions in axial morphology along the Southeast Indian Ridge, *J. Geophys. Res., 101,* 15,849-15,866, 1996.

Mitchell, N. C., A model for attenuation of backscatter due to sediment accumulations and its application to determine sediment thicknesses with GLORIA side-scan sonar, *J. Geophys. Res., 98,* 22,477-22,493, 1993.

Mitchell, N. C., and R. A. Livermore, Spiess Ridge: An axial high on the slow spreading Southwest Indian Ridge, *J. Geophys. Res., 103,* 15,457-15,471, 1998.

Morgan, W. J., Rodriguez, Darwin, Amsterdam,..., a second type of hotspot island, *J. Geophys. Res., 83,* 5355-5360, 1978.

Neumann, G. A , and D. W. Forsyth, The paradox of the axial profile: Isostatic compensation along the axis of the Mid-Atlantic Ridge?, *J. Geophys. Res., 98,* 17,891-17,910, 1993.

Phipps Morgan, J., and Y. J. Chen, Dependence of ridge axis morphology on magma supply and spreading rate, *Nature, 364,* 706-708, 1993.

Pollard, D. D., and A. Aydin, Propagation and linkage of oceanic ridge segments, *J. Geophys. Res., 89,* 10,017-10,028, 1984.

Ribe, N., The dynamics of plume-ridge interaction, 2, Off-ridge plumes, *J. Geophys. Res., 101,* 16,195-16,204, 1996.

Ribe, N., U. R. Christensen, and J. Theissing, The dynamics of plume-ridge interaction, 1, Ridge-centered plumes, *Earth Planet. Sci. Lett., 134,* 155-168, 1995.

Royer, J -Y., and D. T. Sandwell, Evolution of the eastern Indian Ocean since the Late Cretaceous: Constraints from Geosat altimetry, *J. Geophys. Res., 94,* 13,755-13,782, 1989.

Royer, J.-Y., and R. Schlich, Southeast Indian Ridge between the Rodriguez triple junction and the Amsterdam and Saint-Paul Islands: Detailed kinematics for the past 20 m.y., *J. Geophys. Res., 93,* 13,524-13,550, 1988.

Sandwell, D. T , and W. H. F. Smith, Marine gravity anomaly from Geosat and ERS 1 satellite altimetry, *J. Geophys. Res., 102,* 10,039-10,054, 1997.

Scheirer, D., D. Forsyth, K. Johnson, D. Graham, and the Boomerang Leg 6 Scientific Party, The Southeast Indian Ridge near Amsterdam and St. Paul Islands: Results from Boomerang, Leg 6, *RIDGE Events, 7,* 5-9, 1996.

Schilling, J.-G., Iceland mantle plume: Geochemical evidence along Reykjanes Ridge, *Nature, 242,* 565-571, 1973.

Schilling, J.-G., Upper mantle heterogeneities and dynamics, *Nature, 314,* 62-67, 1985.

Schilling, J.-G., Fluxes and excess temperatures of mantle plumes inferred from their interaction with migrating mid-ocean ridges, *Nature, 352,* 397-403, 1991.

Sempere, J.-C., J. R. Cochran, and SEIR Scientific Team, The Southeast Indian Ridge between 88°E and 118°E: Variations in crustal accretion at constant spreading rate, *J. Geophys. Res., 102,* 15,489-15,505, 1997.

Shah, A. K., and J.-S. Sempere, Morphology of the transition from an axial high to a rift valley at the Southeast Indian Ridge and the relation to variations in mantle temperature, *J. Geophys. Res., 103,* 5203-5223, 1998.

Sleep, N. H., Hotspots and mantle plumes: Some phenomenology, *J. Geophys. Res., 95,* 6715-6736, 1990.

Sleep, N., Lateral flow of hot plume material ponded at sublithospheric depths, *J. Geophys. Res., 101,* 28,065-28,083, 1996.

Small, C., and D. T. Sandwell, An abrupt change in ridge axis gravity with spreading rate, *J. Geophys. Res., 94,* 17,383-17,392, 1989.

Storey, M., A. D. Saunders, J. Tarney, I. L. Gibson, M. J. Norry, M. F. Thirlwall, P. Leat, R. N. Thomson, and M. A. Menzies, Contamination of Indian Ocean asthenosphere by the Kerguelen-Heard mantle plume, *Nature, 338,* 574-576, 1989.

Talwani, M., C. C. Windisch, and M. G. Langseth, Reykjanes Ridge crest: A detailed geophysical study, *J. Geophys. Res., 76,* 473-517, 1971.

Upton, B. G. J., Oceanic islands, in *The Ocean Basin and Margins,* vol. 6 *The Indian Ocean,* edited by A. E. M. Nairn and F. G. Stehli, pp. 585-648, Plenum, New York, 1992.

Vogt, P. R., Asthenosphere motion recorded by the ocean floor south of Iceland, *Earth Planet. Sci. Lett., 13,* 153-160, 1971.

Vogt, P. R., Plumes, subaxial pipe flow, and topography along the mid-oceanic ridge, *Earth Planet. Sci. Lett., 29,* 309-325, 1976.

Wessel, P., and W. H. F. Smith, New version of the generic mapping tools released, *Eos Trans. AGU, 76,* 329, 1995.

Yale, M. M., and J. Phipps Morgan, Asthenosphere flow model of hotspot-ridge interactions: A comparison of Iceland and Kerguelen, *Earth Planet. Sci. Lett., 161,* 45-56, 1998.

J. A. Conder, D. W. Forsyth, and D. S. Scheirer, Department of Geological Sciences, Box 1846, Brown University, Providence, RI 02912. (scheirer@emma.geo.brown.edu)

M. A Eberle, Fred Hutchinson Cancer Research Center, P.O. Box 19024, Seattle, WA 98109. (meberle@fhcrc.org)

D. Graham, College of Oceanography and Atmospheric Sciences, Oregon State University, Corvallis, OR 97331. (dgraham@oce.orst.edu)

S-H. Hung, Department of Geosciences, Princeton University, Princeton, NJ 08544. (shung@geo.princeton.edu)

K. T. M. Johnson, Bishop Museum, Natural Sciences, 1525 Bernice St., Honolulu, HI 96817. (kevinj@soest.hawaii.edu)

(Received March 26, 1999; revised August 31, 1999;
accepted November 10, 1999)